

Anisotropic limit of the bond-percolation model and conformal invariance in curved geometriesYoujin Deng¹ and Henk W. J. Blöte^{1,2}¹*Faculty of Applied Sciences, Delft University of Technology, P.O. Box 5046, 2600 GA Delft, The Netherlands*²*Lorentz Institute, Leiden University, P.O. Box 9506, 2300 RA Leiden, The Netherlands*

(Received 29 January 2004; published 17 June 2004)

We investigate the anisotropic limit of the bond-percolation model in d dimensions, which is equivalent to a $(d-1)$ -dimensional quantum $q \rightarrow 1$ Potts model. We formulate an efficient Monte Carlo method for this model. Its application shows that the anisotropic model fits well with the percolation universality class in d dimensions. For three-dimensional rectangular geometry, we determine the critical point as $t_c = 8.6429(4)$, and determine the length ratio as $\alpha_0 = 1.5844(3)$, which relates the anisotropic limit of the percolation model and its isotropic version. On this basis, we simulate critical systems in several curved geometries including a spheroid and a spherocylinder. Using finite-size scaling and the assumption of conformal invariance, we determine the bulk and surface magnetic exponents in two and three dimensions. They are in good agreement with the existing results.

DOI: 10.1103/PhysRevE.69.066129

PACS number(s): 05.50.+q, 64.60.Cn, 64.60.Fr, 75.10.Hk

I. INTRODUCTION

Since their original introduction in 1957 [1], percolation problems have been studied extensively, and a variety of applications has also been reported (see, e.g., Refs. [2,3]). Percolation provides a simple picture of a second-order phase transition, and remains an active research subject [4–6]. We illustrate the problem of the bond percolation on a regular lattice. Between each pair of lattice sites, a bond is occupied or empty with a probability p or $1-p$, respectively. Two sites connected through a chain of occupied bonds are said to be in the same cluster. Then, various questions can be asked concerning the critical cluster distribution and the percolation probability, etc. Such percolation problems are now rather well understood; this can at least partly be attributed to the well-known relationship [7] between the bond percolation and the Potts model (for a review of the Potts model, see Ref. [8]). In this way, the phase transition that occurs in percolation problems can be described in the language of critical phenomena in statistical physics. As a consequence, a considerable number of critical exponents is now exactly obtained in two dimensions. For instance, the thermal and magnetic scaling exponents are $y_t = 3/4$ and $y_h = 91/48$. These exponents can be calculated from the Coulomb gas theory [9,10] and are also predicted by the conformal field theory [11–13].

Besides the above isotropic percolation model, it is of interest to understand the behavior of anisotropic systems in the percolation theory. For instance, an anisotropic random percolation model was demonstrated to be governed by new, random fixed points [14]. In the present paper, we shall consider the anisotropic bond-percolation model, which is defined on a d -dimensional rectangular lattice with a bond probability p_\perp within $(d-1)$ -dimensional layers perpendicular to the z direction, and with the probability $p_\parallel = R p_\perp$ parallel to z . For $R=0$, the system decouples into independent $(d-1)$ -dimensional layers, so that the percolation problem reduces to $(d-1)$ dimensions. Models with a finite and non-zero R have already received some attention [15], and it was

shown that they are within the same universality class as the isotropic percolation model in d dimensions. In the present paper, we shall focus on the limit $R \rightarrow \infty$. In this anisotropic limit of the bond-percolation model, the probability p_\perp in the $(d-1)$ -dimensional layers approaches 0 near criticality, and thus one can express p_\perp and p_\parallel as

$$p_\parallel(p_z) = 1 - \epsilon, \quad \text{and} \quad p_\perp = \epsilon/t \quad (\epsilon \rightarrow 0), \quad (1)$$

where t is a temperaturelike parameter. When ϵ is precisely zero, the system becomes one-dimensional and this percolation problem is trivial. However, as we shall argue later, the anisotropic percolation model defined by Eq. (1) is equivalent with a quantum $q \rightarrow 1$ Potts model in $(d-1)$ dimensions, which fits in the d -dimensional percolation universality class.

For the anisotropic model defined by Eq. (1), the correlation length in the z direction is of the order of $1/\epsilon$. In order to maintain the d -dimensional character of the system, the lattice size in this direction must also diverge as $1/\epsilon$. Thus, we apply a rescaling $z' = z\epsilon$, so that the correlation length in the new unit and the physical size remain approximately constant. As $\epsilon \rightarrow 0$, the z' dimension becomes continuous, and we refer to the resulting continuous percolation problem as the transverse percolation model. A detailed description of the above procedure will be given in Sec. II.

Next, we formulate a Monte Carlo method for the transverse percolation model. The numerical results confirm that the transverse percolation model belongs to the same universality class as the conventional percolation problem on a discrete lattice.

Another purpose of the present paper is the application of conformal mappings in curved geometries. In two dimensions, the theory of conformal invariance has yielded substantial results [11–13]. Conformal mappings yield relations between critical systems in different geometries, and thus provide useful tools for the determination of universal properties of critical models. A well-known example is Cardy's mapping between an infinite plane and the surface of an infinitely long cylinder [16]. Since a cylinder is pseudo-one-

dimensional, its numerical investigation is simpler than that of a two-dimensional plane. Cardy's mapping can be generalized to any number of spatial dimensions, and in three dimensions it transforms an infinite space \mathbb{R}^3 into a pseudo-one-dimensional geometry $S^2 \times \mathbb{R}$. However, the nonzero curvature of the geometry $S^2 \times \mathbb{R}$ poses a serious obstacle for numerical simulations.

In applications to the Ising model, this problem was solved recently in Refs. [17–19]. The solution makes use of the Hamiltonian limit of the lattice Ising model, which renders one of the lattice directions continuous. Thus, one can perform Monte Carlo simulations in curved geometries, such as the surface of a sphere $S^1 \times S^1$ in two dimensions and the cylinderlike geometry $S^2 \times \mathbb{R}^1$ in three dimensions. It was reported [17,18] that, in three dimensions, the Ising model is conformally invariant and the corresponding estimations of critical exponents are compatible with existing results. In Ref. [17] the three-dimensional geometry $S^2 \times \mathbb{R}^1$ was named a spherocylinder. Here, we simulate the transverse percolation model in curved geometries, which provides another application of conformal mappings to investigate bulk and surface critical phenomena.

The outline of this paper is as follows. Section II explores the relationship of the anisotropic limit of the percolation model defined by Eq. (1) and the quantum $q \rightarrow 1$ system in $(d-1)$ dimensions, and moreover a Monte Carlo method is formulated for this anisotropic percolation model. In Sec. III, Monte Carlo simulations in the two- and three-dimensional rectangular geometries are presented. Section IV summarizes the conformal mappings involved in the present paper; applications of these mappings are reported in Sec. V. We give a short discussion in Sec. VI.

II. MODELS AND ALGORITHMS

A. Quantum transverse q -state Potts model

The partition sum of the $q=1$ Potts model is just a constant, so that its equivalence to the bond-percolation model has to be formulated [7] in terms of geometric properties of the random-cluster representation of the Potts model in the limit $q \rightarrow 1$. To explore the anisotropic limit of the bond-percolation model defined by Eq. (1), we start with the Hamiltonian limit of an Ising model on an $N \times M$ rectangular lattice with periodic boundary conditions

$$\mathcal{H}/k_B T = - \sum_{i,j} [K_x s_{i,j} s_{i+1,j} + K_y s_{i,j} s_{i,j+1}]. \quad (2)$$

The spins can assume the values $s_{i,j} = \pm 1$, the integer coordinates i and j label the lattice sites, and K_x and K_y are the coupling strengths in the x and y directions, respectively. The critical line of this model is given by [20]

$$\sinh(2K_x) \sinh(2K_y) = 1. \quad (3)$$

Thus, in the anisotropic limit $\epsilon \rightarrow 0$, the couplings can be written as

$$K_x = \epsilon/t, \quad \text{and} \quad \exp(-2K_y) = \epsilon \quad (\epsilon \rightarrow 0), \quad (4)$$

where t parametrizes the temperature; the critical point is $t_c = 1$.

The Hamiltonian limit of the lattice Ising model defined by Eqs. (2) and (4) can be exactly mapped onto the one-dimensional quantum Ising model [21]. This equivalence was formulated in the reverse direction by Suzuki [22], using the Trotter formula [23]. The Hamiltonian of the quantum Ising chain reads

$$\mathcal{H}_{\text{qm}} = - \sum_i (\sigma_i^z \sigma_{i+1}^z + t \sigma_i^x), \quad (5)$$

where σ^z and σ^x are the Pauli matrices for the z and x spin components, respectively. The Hamiltonian \mathcal{H}_{qm} contains noncommuting operators and represents a quantum system with nearest-neighbor Ising interactions, and the temperaturelike parameter t acts as a transverse field in the x direction.

This equivalence can be readily generalized to spatial dimensions $d > 2$, i.e., the Hamiltonian limit of a d -dimensional lattice Ising model is equivalent with the transverse Ising model in $(d-1)$ dimensions.

Including the transverse Ising model as a special case, one can define a general quantum q -state Potts model [24,25]. For instance, the Hamiltonian of a quantum q -state Potts chain (with integer q) can be written as

$$\mathcal{H}_{\text{qm}} = - \sum_i \sum_{k=0}^{q-1} (S_k^i S_{i+1}^{q-k} + t R_i^k), \quad (6)$$

where S and R are $q \times q$ matrices satisfying the $Z(q)$ algebra

$$[S_i, S_j] = [R_i, R_j] = [S_i, R_j] = 0, \quad i \neq j,$$

$$S_j R_j = \exp(i2\pi/q) R_j S_j, \quad \text{and} \quad R_j^q = S_j^q = I. \quad (7)$$

For the case of $q=2$, the operators S and R reduce to the Pauli matrices σ^z and σ^x , respectively, and Eq. (6) simplifies to Eq. (5). The eigenspectra of these critical quantum q -state Potts chains ($0 < q \leq 4$) with free and periodic boundary conditions have already been explored in Refs. [24,25], and it was shown that, indeed, they share the same critical exponents as the corresponding classical q -state Potts models in two dimensions.

For noninteger q or the limiting case $q \rightarrow 1$, Eqs. (6) and (7) are not suitable to describe the Hamiltonian limit of the q -state Potts model. In this case, one can instead apply the transfer matrix of the random-cluster model [26]. The evaluation of the partition function uses the transfer matrix as

$$Z = \sum_{s^{(1)}, s^{(2)}, \dots} \langle s^{(1)} | \mathbf{T} | s^{(2)} \rangle \dots \langle s^{(y)} | \mathbf{T} | s^{(y+1)} \rangle \dots, \quad (8)$$

where $s^{(y)}$ is the bond configuration at the y th row and the transfer is in the direction of the strong coupling. For the anisotropic bond-percolation model described by Eq. (1), the transfer matrix reads

$$\langle s^{(y)} | \mathbf{T} | s^{(y+1)} \rangle = I - \epsilon \sum_x \left[\mathbf{B}_x^{(y,y+1)} - \frac{1}{t} \mathbf{C}_{x,x+1}^{(y)} \right] + O(\epsilon^2), \quad (9)$$

where I is the unit matrix. The symbol $\mathbf{B}_x^{(y,y+1)}$ represents that, between the y th and $(y+1)$ rows, a ‘‘broken’’ bond oc-

curs at the site x while the remaining bonds are occupied, and $C_{x,x+1}^{(y)}$ means that only *one* bond exists between x and $x+1$ at the y th row. Once q is not precisely equal to 1, the operators \mathbf{B} and \mathbf{C} do not commute, and thus are quantum operators. For $t \ll 1$, most sites are connected so that the system is in an “ordered” state; while for $t \gg 1$, they are independent of each other and the system is “disordered.” A phase transition occurs at $t=1$.

Therefore, we simply expect that the anisotropic limit of the bond-percolation model by Eq. (1) is within the same universality class with the corresponding isotropic version. This will be demonstrated further by means of Monte Carlo simulations.

B. Algorithms

We consider the anisotropic limit of the bond-percolation model [Eq. (1)] on an $N \times M$ rectangular lattice with periodic boundary conditions. The bond occupation probabilities in the x and y directions are p_{\perp} and p_{\parallel} in Eq. (1), respectively. For such a system, the correlation length in the y direction is of order $1/\epsilon$, as mentioned earlier. Thus, we have to take the lattice size M proportional to $1/\epsilon$ while if N is kept constant. Since computer memories are finite, it may not immediately be obvious how a Monte Carlo algorithm can be formulated.

Let us start with the procedures commonly used for the cluster decomposition of the isotropic version of the percolation model with the bond probability p . First, one introduces a bond variable b_{ij} for each bond between nearest-neighbor sites i and j . Occupied and empty bonds are represented by $b_{ij}=1$ and 0, respectively. For each bond variable b_{ij} , one draws a uniformly distributed random number r ($0 \leq r < 1$), and sets $b_{ij}=1$ if $r < p$. The whole lattice is then decomposed into clusters of connected sites through the occupied bonds. These percolation clusters are analogous to the Swendsen-Wang clusters in the Potts model [27].

For the anisotropic limit of the percolation model defined by Eq. (1), the bond probability in the y direction is $p_y=1-\epsilon$, so that one has to draw of order $1/\epsilon$ random numbers r before finding an empty bond $b_y=0$. This indicates that empty bonds are sparsely distributed in the y direction. In the x direction, the bond probability $p_x \propto \epsilon$ so that the task to find the next occupied bond $b_x=1$ again involves of order $1/\epsilon$ random numbers.

A more efficient procedure follows [28]. Counting the bond variables sequentially in the y direction, the distribution $P_y(m) \equiv (1-p_y)p_y^{m-1}$ expresses the probability that $(m-1)$ subsequent bond variables b_{ij} are equal to 1, while the m th variable is zero, i.e., an empty bond occurs at m th position. Thus, the cumulative distribution can be written as

$$C_y(m) = \sum_{j=1}^m P_y(j) = 1 - p_y^m = 1 - (1 - \epsilon)^m, \quad (10)$$

which represents the probability that an empty bond $b_j=0$ occurs in the range $1 \leq j \leq m$. Thus, by mapping the distribution $0 < C_y(m) < 1$ on the uniform distribution of the random number r , one transforms r into an integer m ,

$$m = 1 + [\ln(r)/\ln(1 - \epsilon)], \quad (11)$$

where $0 < r < 1$ and the square brackets denote the integer part of the number in between. The number m represents the distance of the current empty bond to the one to be generated. Thus, only one random number is needed to generate the next empty bond in the y direction.

In the x direction, one instead uses the distribution $P_x(n) \equiv p_x(1-p_x)^{n-1}$ to express the probability that $(n-1)$ subsequent variables b_{ij} are zero, while the n th bond variable is 1. We mention that, although the bond variables are now in the x direction, they are still counted sequentially along the y direction. Analogously, one can transform a uniformly distributed random number r into an integer n ,

$$n = 1 + [\ln(r)/\ln(1 - p_x)] \quad (p_x = \epsilon/t). \quad (12)$$

The average number of the y -dimensional empty bonds and that of the occupied bonds in the x direction are

$$m \equiv \int_0^1 dr \ln(r)/\ln(1 - \epsilon) \propto \frac{1}{\epsilon}, \quad \text{and} \quad n \propto \frac{t}{\epsilon}, \quad (13)$$

respectively. Now, suppose the $N \times M$ square lattice represents a conducting network, and the occupied bonds act as the elementary conducting units. According to Eq. (13), in the y direction, the current is allowed to flow along the conducting “lines” until it occasionally encounters an empty bond, to which we shall refer as a barrier with an infinitely large resistance. In the x direction, since most bonds are empty, the areas between the neighboring conducting lines can be considered to be filled with an insulating material, and the electrical current has to rely on sparsely distributed “bridges” (occupied bonds). If a potential difference is applied to the up and down sides of the $N \times M$ network, the corresponding conductivity of this network then depends on the relative abundance of the bridges and barriers. According to Eq. (13), the average total numbers of the barriers and the bonds are $NM\epsilon$ and $NM\epsilon/t$, respectively, so that they remain finite in the limit $\epsilon \rightarrow 0$. Thus, the conductivity of the network depends only on the temperaturelike parameter t . For $t \gg 1$, the sizes of conducting clusters are small, and the up and down sides are disconnected, so that no current exists; if the temperature t is sufficiently low, a percolating cluster which carries current may occur in the system.

Although one now needs only a finite number of random numbers, one still has to solve the problem of the infinite size M in the y direction, reflected by the divergence of m and n . This can be done by rescaling the y direction as $y' = \epsilon y$, so that the physical size $M' = M\epsilon$ remains approximately a constant. In the limit $\epsilon \rightarrow 0$, the y dimension becomes continuous, i.e., there is an infinite number of lattice sites per physical length unit, and the $N \times M$ square lattice reduces to N lines of physical length M' . Meanwhile, Eqs. (11) and (12) change into

$$m' = \epsilon m = -\ln(r), \quad \text{and} \quad n' = \epsilon n = -t \ln(r) \quad (\epsilon \rightarrow 0), \quad (14)$$

which indicates that the average distances of the barriers and bridges, m' and n' , are now of the order of 1. As a result,

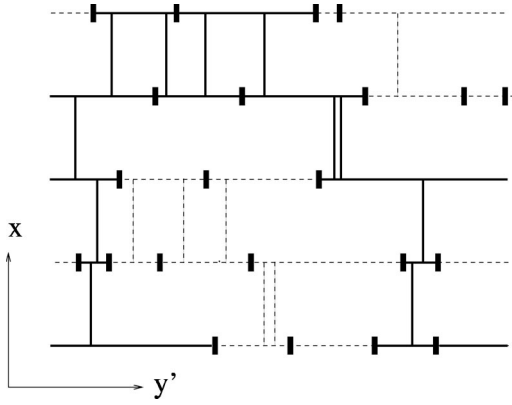


FIG. 1. The anisotropic limit of the percolation model after the rescaling $y' = \epsilon y$. The horizontal lines represent “conducting” lines in the y' direction, and the black bars are barriers with an infinitely large resistance on these lines; the vertical lines serve as “bridges” between neighboring lines. One percolating cluster is shown by solid lines. This figure shows that the conducting lines on the left- and right-hand sides of a barrier may belong to the same cluster, but in that case they are via a detour. If this barrier is removed, the cluster size will remain unchanged.

after the rescaling $y' = y\epsilon$, the anisotropic limit of the percolation model defined by Eq. (1) reduces to a continuous percolation model, to which we shall refer as the transverse percolation model. A typical configuration is shown in Fig. 1, where the horizontal lines are the aforementioned conducting lines and the vertical lines are the bridges in the transverse direction. The black bars represent the barriers, through which the current cannot penetrate. For clarity, in Fig. 1 we have outlined a cluster by means of solid lines.

Conventional Monte Carlo methods for discrete lattice percolation problems store the lattice sites simply in an array. For the transverse percolation, this is no longer applicable, since one of the dimensions is now continuous. However, as mentioned above, the total number of the barriers and bridges still remains finite, so that one can make use of their positions as the dynamical variables. On this basis, a procedure for the cluster decomposition and the sampling is formulated as follows.

First, *randomly distribute barriers and bridges over the $N \times M'$ geometry*. Starting from an arbitrarily chosen origin, the positions of the barriers and the bridges are sequentially generated by Eq. (14). For instance, suppose the current Monte Carlo step arrives at the i th barrier, whose position is stored as (x_i, y_i) . Here, the coordinates (x_i, y_i) represent that the i th barrier sits at the position y_i of the x_i th line. Then, one draws a random number $0 < r < 1$ and evaluates m' by Eq. (14). If $y_i + m' \leq M'$, the $(i+1)$ th barrier is placed at the same line as the i th one, and thus $x_{i+1} = x_i$ and $y_{i+1} = y_i + m'$; otherwise if $M' < y_i + m' \leq 2M'$, the $(i+1)$ th barrier is at $(x_i + 1, y_i + m' - M')$; ... Repeat this procedure until the whole $N \times M'$ geometry is visited. The same procedure is applied to the distribution of the bridges, and the total numbers of the barriers and the bridges are denoted as B_l and B_r , respectively.

Second, *sample the sizes of the clusters*. After the first step, the geometry is now decomposed into clusters which

consists of conducting lines connected through the bridges. The size of the i th cluster is the sum of the lengths of the conducting lines in it, which can be calculated from the positions of the barriers stored in the computer memory. If the size of the i th cluster is denoted as S_i , a quantity resembling the magnetic susceptibility χ and the corresponding Binder-like ratio Q [29] can be defined as

$$\chi = \frac{1}{V} \left\langle \sum_i S_i^2 \right\rangle \equiv V \langle m^2 \rangle, \quad \text{and} \quad Q = \frac{\left\langle \left(\sum_i S_i^2 \right)^2 \right\rangle}{\left(\sum_i S_i^2 \right)^2}, \quad (15)$$

where $V \equiv NM'$ is the volume of the system.

During the first step of the above algorithm, the function, $\ln r$, has to be frequently carried out, which decreases somewhat the efficiency of the algorithm. A different procedure can be applied as follows. From Eq. (14), the total number of the barriers and bridges is as $\langle B_l \rangle = V / \langle m' \rangle = V$ and $\langle B_r \rangle = V / \langle n' \rangle = V/t$, respectively. Instead of allowing the fluctuations of B_l and B_r during Monte Carlo simulations, one may fix them at their expectation values V and V/t , respectively. Since these barriers and bridges are uniformly distributed, their positions can now be *independently* calculated as $l_i = rV$ with the random number $0 < r < 1$. Then, the coordinates of the i th barrier is given by $x_i = [l_i / M'] + 1$ and $y_i = l_i - (x_i - 1)M'$, where the square brackets represent the integer part. Here, the word “independently” means that the position of the $(i+1)$ th barrier does not depend on that of the i th one.

However, in this way, since the fluctuations of the energylike quantities B_l and B_r are suppressed, an external constraint is effectively imposed on the system. A question arises how this energylike constraint affects the critical behavior of the system. For the percolation model, since the thermal scaling exponent satisfies $2y_t - d < 0$, it can be shown [30] that the leading scaling behavior of the critical system is not modified. But new corrections to scaling can arise due to this constraint. To avoid this complication, we still use Eq. (14) to generate positions of the barriers and bridges in the present paper.

III. SIMULATIONS IN FLAT GEOMETRIES

A. Two dimensions

For the anisotropic limit of the percolation model in the two-dimensional rectangular geometry, the duality argument yields that the critical point is $t_c = 1$, since the critical bond probabilities satisfy $p_{xc} + p_{yc} = 1$. Furthermore, the thermal and magnetic critical exponents are exactly known, as mentioned earlier. Thus, this model provides a good test case for the Monte Carlo algorithm described in Sec. II and the universality of the transverse percolation model.

The simulations used a rectangular geometry of L lines of length L in the range $6 \leq L \leq 32$. Periodic boundary conditions were applied, and the dimensionless Binder-like ratio Q and the susceptibilitylike quantity χ defined in Eq. (15) were sampled. Near the critical point, the numerical data of Q were fitted [31] by

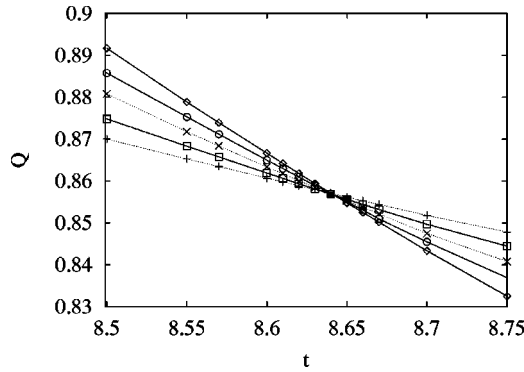


FIG. 2. The Binder-like ratio Q vs the temperaturelike parameter t for the transverse percolation model on the $L^2 \times L$ rectangular geometry. The system size L is 12 (+), 16 (□), 20 (×), 24 (○), and 28 (◻), respectively.

$$Q(t, L) = q_0 + \sum_{k=1}^4 q_k (t - t_c)^k L^{ky_t} + b_1 L^{y_1} + b_2 L^{y_2} + c_1 (t - t_c) L^{y_t + y_1}. \quad (16)$$

The terms with $y_1 = -2$ and $y_2 = -3$ account for corrections to scaling. The fit with $y_t = 3/4$ yields $t_c = 0.9994(5)$, in good agreement with the exact result $t_c = 1$. If t_c is kept fixed at 1 while y_t is left free, we have $y_t = 0.752(3) \approx 3/4$ [9–13]. Moreover, we fitted the Monte Carlo data of χ at $t_c = 1$ by the formula

$$\chi(t_c) = x_0 + L^{2y_h - 2} (b_0 + b_1 L^{y_1} + b_2 L^{y_2}), \quad (17)$$

from which we obtain $y_h = 0.1043(4) \approx 5/48$ [9–13].

B. Three dimensions

As mentioned earlier, three-dimensional percolation models have been investigated extensively [2–6]. The most accurate results are provided by Monte Carlo simulations. For instance, for the isotropic bond-percolation model on the simple-cubic lattice, the percolation threshold is estimated [4] as $p_c = 0.248\,821\,6(5)$; the thermal and magnetic exponents are reported [4] as $y_t = 1.13(2)$ and $y_h = 2.523(4)$, respectively.

Using the aforementioned Monte Carlo algorithm, we simulated the transverse percolation model on the three-dimensional rectangular geometry: L^2 lines of length L originating from the $L \times L$ square lattice. The system sizes are in the range $6 \leq L \leq 40$, periodic boundary conditions were applied, and the quantities Q and χ in Eq. (15) were sampled. Part of the data for Q is shown in Fig. 2, indicating that the critical point is located at $t_c \approx 8.64$. The clean intersection of these lines suggests that corrections to scaling are rather small. Equation (16) was fitted to the data of Q , with y_1 and y_2 taken as -1.14 and -2 [4], respectively. For y_t fixed at 1.13, we obtain $t_c = 8.6428(2)$; if y_t is left free, we find $y_t = 1.135(8)$ and $t_c = 8.6429(4)$, with the error margin twice the standard deviation.

Moreover, the data for χ were fitted by [31]

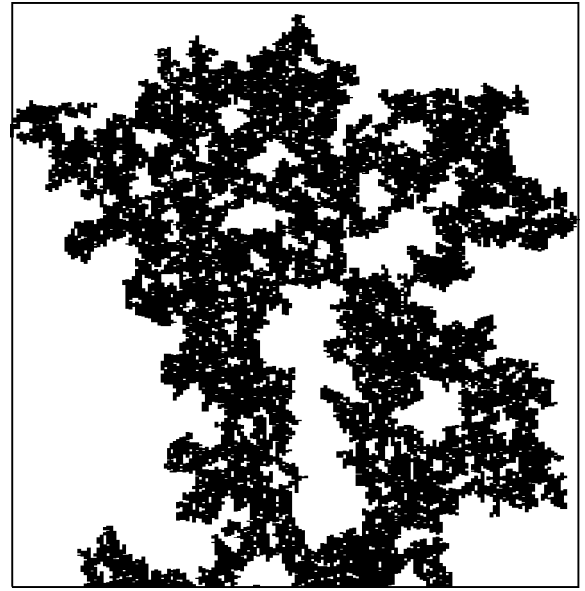


FIG. 3. A cluster for the transverse percolation model on the $L \times L$ rectangular geometry with free boundary conditions and $L = 100$.

$$\chi = x_0 + x_1 (t - t_c) + x_2 (t - t_c)^2 + L^{2y_h - 2} \times \left[\sum_{k=1}^4 a_k (t - t_c)^k L^{ky_t} + b_1 L^{y_1} + b_2 L^{y_2} + c_1 (t - t_c) L^{y_t + y_1} \right], \quad (18)$$

where the terms with x_i ($i = 0, 1, 2$) arise from the regular part of the free energy. With the thermal exponent $y_t = 1.13$, we obtain $y_h = 2.519(1)$, where the estimated error margin includes the uncertainty of y_t .

These investigations confirm the correctness of the Monte Carlo algorithm described in Sec. II, and moreover confirm that the transverse percolation model belongs to the same universality class as the isotropic version of the percolation model on discrete lattices.

C. Restoration of isotropy

Although the transverse percolation model defined by Eq. (1) is intrinsically anisotropic, the correlation lengths in the longitudinal and transverse directions are of the same order. This can be demonstrated by the approximate isotropy of a cluster in Fig. 3. This arises from the rescaling $z' = \epsilon z$ in the longitudinal direction discussed in Sec. II. In fact, one can asymptotically restore the isotropy by choosing an appropriate rescaling factor, i.e., $z' = \epsilon z / \alpha_0$ with α_0 a constant. The value of α_0 is important in the present investigation, since we are also interested in applications of conformal mappings, which rely on isotropy.

In two dimensions, we simulated the transverse percolation model precisely at $t_c = 1$ on the $L \times L$ rectangular geometry. The system sizes and the length ratio were taken as in the range $6 \leq L \leq 64$ and $0.65 \leq \alpha \leq 0.80$, respectively. Free boundary conditions were applied both in the x and y directions. During the Monte Carlo simulations, we sampled the

percolation probabilities in both directions, denoted as P_x and P_y . Accordingly, we define a dimensionless ratio

$$r(\alpha, L) = \left\langle \frac{P_x}{P_y} \right\rangle. \quad (19)$$

Thus, the aforementioned isotropy means $r(\alpha_0, L) = 1$. Taking into account finite-size effects, we fitted the data of $r(\alpha, L)$ by

$$r(\alpha, L) = 1 + a_1(\alpha - \alpha_0) + a_2(\alpha - \alpha_0)^2 + \cdots + b_1 L^{y_1} + b_2 L^{y_2} + c_1 L^{y_1}(\alpha - \alpha_0). \quad (20)$$

The terms with y_1 and y_2 describe corrections to scaling, due to small-scale deviations from isotropy of the transverse percolation model. The numerical data can be successfully described by Eq. (20) with $y_1 = -2$ and $y_2 = -3$, and the fit yields $\alpha_0 = 0.76978(7)$, in agreement with the number $4/3\sqrt{3}$ [25].

Similarly, for the three-dimensional rectangular geometry $L^2 \times L$ with free boundary conditions, one can define the ratio $r(\alpha, L)$ on the basis of the percolation probabilities in the discrete and continuous directions. Simulations were performed at the aforementioned estimated critical point $t_c = 8.6429(4)$, and the system sizes were taken in the range $6 \leq L \leq 40$. The data of $r(\alpha, L)$ were fitted by Eq. (20) with $y_i = -1.14$ [4]. After a cutoff for small system sizes $L \leq 10$, the fit yields $\alpha_0 = 1.5844(4)$.

IV. CONFORMAL INVARIANCE

In this section, we summarize the conformal mappings and the corresponding transformations of the pair correlation functions involved in the present paper. Most of these mappings have already been derived in Refs. [13,16–18].

A. Spherocylinder

In two dimensions, one may parametrize the infinite plane as a complex number $z = x + iy$, Cardy's well-known mapping [13,16] is then expressed as $z' = R \ln z$. The geometry z' can be interpreted as the surface of an infinitely long cylinder $S^1 \times \mathbb{R}^1$ with a radius R . This mapping can be generalized to any number of dimensions. For instance, in spherical coordinates (r, θ, ϕ) , Cardy's mapping in three dimensions reads

$$(r, \theta, \phi) = (e^{u/R}, \theta, \phi) \quad (-\infty < u < \infty) \quad (21)$$

with $R > 0$ a free parameter. The geometry described by the variables (u, θ, ϕ) has a line element as

$$ds^2 = du^2 + R^2(d\theta^2 + \sin^2 \theta d\phi^2) \quad (0 \leq \theta \leq \pi, 0 \leq \phi < 2\pi) \quad (22)$$

and thus can be recognized as the extension of a sphere S^2 into another dimension \mathbb{R} . In Ref. [17], this pseudo-one-dimensional geometry $S^2 \times \mathbb{R}$ was named a spherocylinder.

In the infinite flat space \mathbb{R}^3 , a critical two-point correlation function $g(r)$ behaves as

$$g(r)_{\mathbb{R}^3} \propto r^{-2X} \quad (r \gg 0), \quad (23)$$

where X is the appropriate scaling dimension. Under the conformal mapping (23), this algebraic decay [Eq. (23)] is covariantly transformed into

$$g(u)_{S^2 \times \mathbb{R}} \propto R^{-2X} (e^{u/2R} - e^{-u/2R})^{-2X}, \quad (24)$$

where $u > 0$ is the distance between a pair of points on the spherocylinder, (u_0, θ, ϕ) and $(u_0 + u, \theta, \phi)$. For $u \gg 0$, the correlation function decays exponentially: $g(u) \propto R^{-2X} e^{-Xu/R} \equiv R^{-2X} e^{-u/\xi}$, so that the correlation length along the spherocylinder is equal to $\xi = R/X$.

B. Interior of a sphere

In two dimensions, the complex function $z' = (z - i)/(z + i)$ [13] maps the infinite plane onto itself, and meanwhile transforms the semi-infinite plane $\mathbb{R} \times \mathbb{R}^+$ into the interior of a unit circle. In fact, such a mapping can be generalized to spatial dimensions $d > 2$. It then reads

$$\vec{r}'/r'^2 = \vec{r}/r^2 + \hat{I}/2, \quad (25)$$

with \hat{I} an arbitrary fixed unit vector. Under Eq. (25), the infinite flat space \mathbb{R}^d is mapped onto itself, and the plane $\hat{I} \cdot \vec{r} = 0$, which corresponds to a spherical surface with an infinite radius, is conformally transformed into the surface of a d -dimensional unit sphere with the center at \hat{I} . The half spaces $\hat{I} \cdot \vec{r} > 0$ and $\hat{I} \cdot \vec{r} < 0$ are transformed into the interior and exterior of this unit sphere, respectively.

On the basis of the conformal transformation (25), it can be shown [13,32] that, in the interior of a sphere with free or fixed boundary conditions, the profile of an operator $\langle \psi \rangle$ follows from

$$\langle \psi(r) \rangle \propto R^{-X} [1 - (r/R)^2]^{-X}, \quad (26)$$

where R is the radius of the sphere.

Furthermore, Eq. (21) transforms the interior of a unit sphere S^d into a semi-infinite spherocylinder $S^{d-1} \times \mathbb{R}^+$, with an end at $u = 0$. Thus, a conformal mapping between the semi-infinite flat space $\mathbb{R}^{d-1} \times \mathbb{R}^+$ and the half spherocylinder $S^{d-1} \times \mathbb{R}^+$ is established, and the profile (26) is covariantly transformed into

$$\langle \psi(u) \rangle \propto R^{-X} (e^{u/2R} - e^{-u/2R})^{-2X}, \quad (27)$$

which differs from Eq. (24) only by a factor R^{-X} .

C. Surface of a sphere

By rotating an ellipse about the minor or major axis, one obtains an oblate or a prolate spheroid, respectively. In three-dimensional Cartesian coordinates (x, y, z) , these spheroids are defined by

$$\frac{x^2}{a^2} + \frac{y^2}{a^2} + \frac{z^2}{b^2} \quad (a, b > 0), \quad (28)$$

where a and b are the equatorial and the polar radii, respectively. Special cases of the spheroids include the surface of

an infinitely long cylinder, of a sphere, and of a flat disc. The latter object is reached in the limit of an oblate spheroid $b \rightarrow 0$. It is already known [18] that a conformal transformation exists between the infinite plane \mathbb{R}^2 and the surface of a spheroid. For simplicity, we here only introduce the mappings of the infinite plane on the surface of a sphere and on that of a flat disc. Further, we generalize such conformal mappings to spatial dimensions $d > 2$.

The transformation between an infinite plane \mathbb{R}^2 and the surface of a sphere S^2 can be graphically understood as follows. A sphere with radius R is placed on the top of an infinite plane, i.e., only the south ‘‘pole’’ of the sphere touches the plane. From the north pole, one draws an arbitrary line, such that this line penetrates through the sphere at \vec{R} and intersects with the plane at \vec{r} . The conformal transformation is simply obtained by setting a one-to-one correspondence between the points \vec{r} and \vec{R} . If one expresses the plane in polar coordinates (r, ϕ) , while parametrizes the surface of the sphere in spherical coordinates $(r=R, \theta, \phi)$, the transformation reads

$$(r, \phi) = \left(2R \cot \frac{\theta}{2}, \phi \right). \quad (29)$$

According to Eqs. (23) and (29), the pair correlation function $g(\vec{R}_1, \vec{R}_2)$ on the sphere follows from

$$g(\vec{R}_1, \vec{R}_2) \propto 2^{-X} R^{-2X} [1 - \sin \theta_1 \sin \theta_2 \cos(\phi_1 - \phi_2) - \cos \theta_1 \cos \theta_2]^{-X} = |\vec{R}_1 - \vec{R}_2|^{-2X}, \quad (30)$$

which, interestingly, has the same form as that in the infinite plane described by Eq. (23).

Application of Eq. (29) to the interior of a unit circle leads to the half sphere $S \times S^+$, so that a conformal transformation between the semi-infinite plane $\mathbb{R} \times \mathbb{R}^+$ and the half surface of a sphere is established. Accordingly, the profile of an operator in the geometry $S \times S^+$ behaves as

$$\langle \psi(\vec{R}) \rangle \propto (R \cos \theta)^{-X}. \quad (31)$$

In spherical coordinates (r, Ω) , where Ω is a set of angular variables specifying the surface of a d -dimensional sphere, the line element of the flat space \mathbb{R}^d can be written as

$$ds^2 = dr^2 + r^2 d\Omega^2. \quad (32)$$

In three dimension, one simply has $d\Omega^2 = d\theta^2 + \sin^2 \theta d\phi^2$. On this basis, one can express the line element of the $(d+1)$ -dimensional space \mathbb{R}^{d+1} as

$$ds'^2 = dr'^2 + r'^2 (d\theta'^2 + \sin^2 \theta' d\Omega'^2). \quad (33)$$

It is now obvious that, for $d > 2$, the generalization of Eq. (29) reads

$$(r, \Omega) = \left(2R \cot \frac{\theta'}{2}, \Omega \right), \quad \text{with } r' = R. \quad (34)$$

Therefore, Eq. (34) transforms an infinite space \mathbb{R}^d into the surface of a $(d+1)$ -dimensional sphere S^d , on which the pair correlation function follows from Eq. (30).

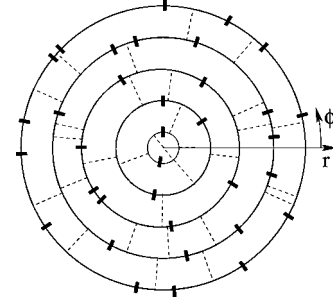


FIG. 4. Example of transverse percolation model on the interior of a circle.

D. Surface of a hyper-disc

As mentioned earlier, the disc geometry is obtained in the limit $b \rightarrow 0$ of an oblate spheroid, composed of the interiors of two circles connected at their perimeters. This can be generalized to $d > 2$, and the surface of a hyperdisc consists of the interiors of two d -dimensional spheres with the surfaces of both spheres sewn together. Then, the conformal mapping between the space \mathbb{R}^d and the surface of the hyperdisc reads

$$\begin{cases} (r, \Omega) = (r'/R, \Omega) & (0 \leq r < 1, \quad r' \leq R: \text{positive face}) \\ (r, \Omega) = (R/r', \Omega) & (0 \leq r < 1, \quad r' \leq R: \text{negative face}). \end{cases} \quad (35)$$

The first derivative of the mapping formula (35) is discrete at the edge of the hyperdisc ($r' = R$). For a pair of points on the same face of the hyperdisc, \vec{r}'_1 and \vec{r}'_2 , the correlation function has the same form as that in the infinite space \mathbb{R}^d , i.e., $g(\vec{r}'_1, \vec{r}'_2) \propto |\vec{r}'_1 - \vec{r}'_2|^{-2X}$.

V. SIMULATIONS IN CURVED GEOMETRIES

As seen from Sec. IV, for spatial dimensions $d > 2$, conformal mappings normally lead to a curved space or a geometry with curved boundaries. Even in two dimensions, curved geometries, such as the surface of a sphere, can also be obtained from conformal transformations. The nonzero curvature of these geometries poses a serious problem for numerical applications of conformal mappings, since they defy discretizations into regular lattices. As a consequence, the validity of Cardy’s mapping was verified only for the special case of the spherical model [33]. Recently, for the case of the Ising model, this difficulty was avoided by making use of the Hamiltonian limit of the Ising model [17,18], which renders one of the dimensions continuous. Since the aforementioned transverse percolation model also has one continuous dimension, we here provide further applications of conformal mappings to both the bulk and surface criticality.

A. Monte Carlo methods in curved geometries

As an example, we sketch a procedure for cluster decomposition of the interior of a circle. First, one divides the geometry into L concentric circles, with the L th circle precisely at the edge (Fig. 4). The location of the k th circle reads r_k

$=k-1/2$, with the corresponding circumference $c_k=\pi(2k-1)$. Then, let the continuous longitudinal dimension of the transverse percolation model be the ϕ direction, so that those concentric circles just represent the conducting lines mentioned above. Then, according to Eq. (14), one generates and uniformly distributes barriers at the concentric circles. We mention that, at the k th circle, the average number of the barriers is controlled by the length of its perimeter. The distribution of bridges follows an analogous way, but the total number of the bridges between the k th and $(k+1)$ th circles ($1\leq k\leq L-1$) is now governed by the circumference of the circle in the middle. Furthermore, the diameter of the first circle is 1, and thus bridges can exhibit through the center, connecting different parts of the first circle. A typical configuration is shown in Fig. 4, where the bridges are denoted as the dashed lines.

Similarly, the “lattice” structure on a sphere S^2 can be represented by L uniformly distributed circles with radii as chosen above. The transverse and longitudinal dimensions are the θ and ϕ directions, respectively. The location of the k th circle is $\theta_k=(k-1/2)\pi/L$, and its circumference is $c_k=2L\sin\theta_k$. Thus, the radius of the sphere is $R=L/\pi$. Analogously, the number of the barriers at the k th circle is dominated by the length of its perimeter, while that of the bridges is governed by the circumference of the circle in the middle of the k th and $(k+1)$ th ones.

On a microscopic scale, the lattice structure on a sphere or the interior of a circle is the same as that on a flat plane, i.e., both of them are obtained in the anisotropic limit of the square lattice. Thus, one expects that the critical point is still $t_c=1$. However, a global effect may arise due to the fact that the nonzero curvature cannot be fully accounted for by circles with varying radius. This has been investigated in Ref. [18], and it was argued that such a global effect can be described by a correction term proportional to L^{y_r-2} . Since the two- and three-dimensional percolation models have $y_t<2$, this effect vanishes as $L\rightarrow\infty$.

It is now obvious that, in three dimensions, the spherocylinder $S^2\times\mathbb{R}$ can be obtained by extending the aforementioned lattice structure of a sphere into another dimension. Meanwhile, in order to approximate the pseudo-one-dimensional geometry of the spherocylinder, the size of the \mathbb{R} direction should be taken as nL with a sufficiently large integer n .

B. Numerical results

With the Monte Carlo algorithms described above, we are now able to simulate the transverse percolation model in the following curved geometries in two and three dimensions.

1. Surface of a sphere

The system sizes were taken in the range $8\leq L\leq 48$, with L the number of circles on the sphere. The simulations occur precisely at the critical point $t_c=1$, and the rescaling length ratio was set at $\alpha_0=0.76978$, such that the isotropy of the transverse percolation is asymptotically restored. We sampled the pair connectivity $P_2(\theta)$ of the points (θ, ϕ) and

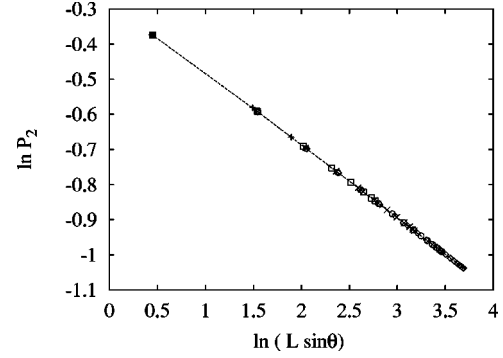


FIG. 5. Data collapse of the quantity $P_2(\theta, L)$ for the transverse percolation model on the sphere. The system sizes are 8 (+), 16 (\square), 24 (\times), 32 (\circ), and 40 (\diamond).

$(\theta, \phi\pm\pi)$ on the same circle. For both points in the same cluster, we say $P_2=1$; otherwise $P_2=0$. According to Eq. (30), the connectivity behaves as $\langle P_2(\theta) \rangle \propto (L\sin\theta)^{-2X_h}$ with X_h the magnetic scaling dimension, graphically shown in Fig. 5. The good quality of the data collapse for different system sizes (Fig. 5) indicates that corrections to scaling are relatively small. The data for P_2 were fitted by

$$\langle P_2(\theta) \rangle = (L\sin\theta)^{-2X_h+cL^{y_c}} [a_0 + a_2L^{y_c} + a_3(L\sin\theta)^{y_c} + \dots], \quad (36)$$

where the exponent $y_c=y_t-2=-5/4$, as explained above. For finite systems, the Hamiltonian may deviate from that at the fixed point, and we account for this by the terms with coefficients c and a_2 . Furthermore, we also include a term with a_3 , describing the inhomogeneity of a finite sphere. We found that the numerical data for $L\geq 12$ are successfully explained by Eq. (36), and the term cL^{y_c} cannot be well observed. The fit with $c=0$ yields $X_h=0.10418(4)$, in good agreement with the exact result $X_h=5/48=0.104167\dots$

2. Interior of a circle

For the Ising model, the geometry inside a circle can be approximated [34] by drawing a circle on the square lattice. Applications of free or fixed boundary conditions are realized by removing or freezing the spins outside the circle, respectively. However, the symmetry along the ϕ direction is broken in this way, and thus irregular finite-size effects arise. The aforementioned Monte Carlo algorithm avoids this difficulty. The system sizes were taken in the range $6\leq L\leq 48$, and fixed boundary conditions were imposed: the whole edge is set within the same cluster. The fraction of the k th circle in this cluster $P_1(r)$ was sampled. The numerical data of $P_1(r)$ were fitted by Eq. (26) but with additional terms accounting for corrections to scaling. We obtain $X_h=0.10413(4)\approx 5/48$.

3. Spherocylinder $S^2\times\mathbb{R}$

The systems were taken as $L=5, 7, \dots, 21$, and the finite-size in the \mathbb{R} direction was set as $nL=8L$. Fixed boundary conditions were imposed at both ends $u=0$ and $u=8L$. The simulations were performed at the estimated critical point $t_c=8.6429$, and the length rescaling ratio was fixed at α_0

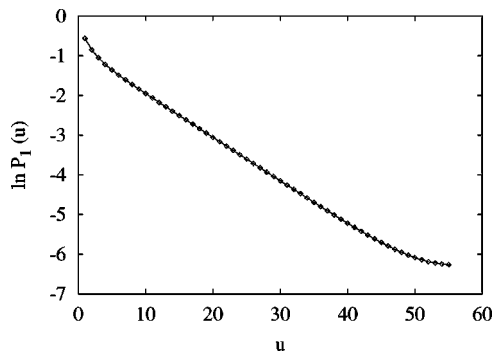


FIG. 6. Exponential decay of $P_1(u)$ along the spherocylinder for the transverse percolation model. The system size is $L=14$ and $n=8$.

$=1.5844$. The quantity $P_1(u)$ was sampled at the “equators” only, in order to avoid inhomogeneity on finite spheres. The behavior of $P_1(u)$ follows from Eq. (27), decaying exponentially for $u \gg 0$. This is demonstrated in Fig. 6. The curved positions at the right-hand side arise because fixed boundary conditions were applied at both ends, so that the correlations $P_1(u)$ build up over two distances u and $8L-u$.

As discussed above, there is a correction $\propto L^{y_c}$ in finite systems, due to the discretization of the θ direction. Compared to the irrelevant scaling exponent $y_i = -1.14$ in three dimensions, the correction with the exponent $y_c = y_i - 2 = -0.87$ is expected to dominate over that with y_i . Taking into account these effects, Eq. (27) yields

$$P_1(u, L) = L^{-X} [Y(u) + Y(8L - u)] (a_0 + a_1 L^{y_c} + a_2 L^{y_i} + a_3 L^{-2}), \quad (37)$$

with the function

$$Y(u) = (e^{uX/2R} - e^{-uX/2R})^{-2X} \quad (X = X_h + cL^{y_c}), \quad (38)$$

where the radius of the spheres is $R = L\pi$ as mentioned earlier.

Equations (37) and (38) were fitted to the Monte Carlo data of $P_1(u)$. The fit yields $X_h = 0.479(1)$, which is in agreement with the existing estimation $y_h = 2.523(4)$ [4] and with our earlier determination $y_h = 2.519(1)$ on the $L^2 \times L$ rectangular geometry.

4. Half spherocylinder $S \times S^+ \times R$

As an example of the applications of conformal mappings to surface criticality, we simulated the transverse percolation model on the half spherocylinder $S \times S^+ \times R$. The system sizes were taken as 6, 8, ..., 24, and $n=8$. The fixed and free boundary conditions were imposed on the ends of the spherocylinder and the equators, respectively. The quantity $P_1(u)$ was sampled. Analogously, the numerical data of $P_1(u)$ were fitted by Eqs. (37) and (38), but $X = X_{hs} + cL^{y_c}$, where X_{hs} is now the surface magnetic scaling dimension. After a cutoff for small system sizes $L \leq 10$, the fit yields $X_{hs} = 0.975(4)$, in good agreement with the existing results $X_{hs} = 0.96(5)$ [35] and $X_{hs} = 0.970(6)$ [36].

VI. DISCUSSION

We define a continuous percolation model: the transverse percolation model. This model is obtained by applying an infinite rescale factor to the longitudinal direction of the anisotropic limit of the bond-percolation model, and is equivalent with the quantum transverse $q \rightarrow 1$ Potts model. We formulate and apply an efficient Monte Carlo method, and confirm that the transverse percolation model belongs to the same universality class as the conventional percolation problem on discrete lattices. For the two-dimensional rectangular geometry, the critical point is exactly available as $t_c = 1$, and that in the three-dimensional rectangular geometry is determined as $t_c = 8.6429(4)$. Furthermore, we restore the isotropy asymptotically by requiring that the correlation lengths in all Cartesian directions are identical to each other.

Moreover, the property that the longitudinal direction is continuous enables simulations of the transverse percolation model in curved geometries. The numerical data are analyzed by finite-size scaling according to the predictions of the theory of conformal invariance. It is shown that, in curved geometries, the predictions of conformal invariance are accurately satisfied. On the other hand, assuming conformal invariance, our method provides a powerful tool to investigate bulk and surface critical phenomena.

ACKNOWLEDGMENT

This research was supported by the Dutch FOM foundation (Stichting voor Fundamenteel Onderzoek der Materie) which is financially supported by the NWO (Nederlandse Organisatie voor Wetenschappelijk Onderzoek).

[1] S. R. Broadbent and J. M. Hammersley, Proc. Cambridge Philos. Soc. **53**, 629 (1957).
 [2] D. Stauffer and A. Aharony, *Introduction to Percolation Theory* (Taylor and Francis, London, 1992), and references therein.
 [3] M. Sahimi, *Applications of Percolation Theory* (Taylor and Francis, London, 1994).
 [4] C. D. Lorenz and R. M. Ziff, Phys. Rev. E **57**, 230 (1997).
 [5] G. Paul, R. M. Ziff, and H. E. Stanley, Phys. Rev. E **64**, 026115 (2001).

[6] C. K. Hu, J. A. Chen, N. S. Izmailian, and P. Kleban, Comput. Phys. Commun. **126**, 77 (2000).
 [7] P. W. Kasteleyn and C. M. Fortuin, J. Phys. Soc. Jpn. **26**, 11 (1969).
 [8] See, e.g., F. Y. Wu, Rev. Mod. Phys. **54**, 235 (1982).
 [9] B. Nienhuis, J. Phys. A **15**, 199 (1982).
 [10] B. Nienhuis, in *Phase Transitions and Critical Phenomena*, edited by C. Domb and J. L. Lebowitz (Academic Press, London, 1987), Vol. 11, p. 1, and references therein.
 [11] A. A. Belavin, A. M. Polyakov, and A. B. Zamolodchikov, J.

- Stat. Phys. **34**, 763 (1984).
- [12] D. Friedan, Z. Qiu, and S. Shenker, Phys. Rev. Lett. **52**, 1575 (1984).
- [13] J. L. Cardy, in *Phase Transitions and Critical Phenomena*, edited by C. Domb and J. L. Lebowitz (Academic Press, London, 1987), Vol. 11, p. 55.
- [14] R. Juhász and F. Iglói, Phys. Rev. E **66**, 056113 (2002).
- [15] S. Redner and H. E. Stanley, J. Phys. A **12**, 1267 (1979).
- [16] J. L. Cardy, J. Phys. A **17**, L385 (1984).
- [17] Y. Deng and H. W. J. Blöte, Phys. Rev. Lett. **88**, 190602 (2002).
- [18] Y. Deng and H. W. J. Blöte, Phys. Rev. E **67**, 036107 (2003); **67**, 066116 (2003).
- [19] H. W. J. Blöte and Y. Deng, Phys. Rev. E **66**, 066110 (2002).
- [20] L. Onsager, Phys. Rev. **65**, 117 (1944).
- [21] T. D. Schultz and D. C. Mattis, Rev. Mod. Phys. **36**, 856 (1964).
- [22] M. Suzuki, Prog. Theor. Phys. **46**, 1337 (1971); *ibid.* **56**, 2454 (1976).
- [23] H. F. Trotter, Proc. Am. Math. Soc. **10**, 545 (1959).
- [24] C. J. Hamer, J. Phys. A **14**, 2981 (1981).
- [25] F. C. Alcaraz, M. N. Barber, and M. T. Batchelor, Phys. Rev. Lett. **58**, 771 (1987); F. C. Alcaraz, M. N. Barber, M. T. Batchelor, and R. J. Baxter, J. Phys. A **20**, 6397 (1987).
- [26] L. Mittag and H. J. Stephen, J. Math. Phys. **12**, 441 (1971); J. Sólyom and P. Pfeuty, Phys. Rev. B **24**, 218 (1981); J. Kogut, Rev. Mod. Phys. **51**, 659 (1979).
- [27] R. H. Swendsen and J.-S. Wang, Phys. Rev. Lett. **58**, 86 (1987); J.-S. Wang and R. H. Swendsen, Physica A **167**, 565 (1990).
- [28] E. Luijten and H. W. J. Blöte, Int. J. Mod. Phys. C **6**, 359 (1995).
- [29] K. Binder, Z. Phys. B: Condens. Matter **43**, 119 (1981).
- [30] M. E. Fisher, Phys. Rev. **176**, 257 (1968).
- [31] H. W. J. Blöte, E. Luijten, and J. R. Heringa, J. Phys. A **28**, 6289 (1995); Y. Deng and H. W. J. Blöte, Phys. Rev. E **68**, 036125 (2003).
- [32] T. W. Burkhardt and E. Eisenriegler, J. Phys. A **18**, L83 (1985).
- [33] J. L. Cardy, J. Phys. A **18**, L757 (1985).
- [34] R. Badke, V. Rittenberg, and H. Ruegg, J. Phys. A **18**, L867 (1985); I. Reš and J. P. Straley, Phys. Rev. B **61**, 14425 (2000).
- [35] A. Hansen, P. M. Lam, and S. Roux, J. Phys. A **22**, 2635 (1989).
- [36] P. Grassberger, J. Phys. A **25**, 5867 (1992).